A nonequilibrium synchrotron X-ray study of a liquid crystal phase transition under shear flow

1990 J. Phys.: Condens. Matter 2 SA365

(http://iopscience.iop.org/0953-8984/2/S/057)

J. Phys.: Condens. Matter **2** (1990) SA365–SA371. Printed in the UK

A non-equilibrium synchrotron x-ray study of a liquid crystal phase transition under shear flow

C R Safinya†, E B Sirota†, R Plano† and R F Bruinsma‡

† Exxon Research and Engineering Company, Route 22 East, Annandale, NJ 08801, USA

‡ Department of Physics, University of California, Los Angeles, CA 90024, USA

Abstract. We report on synchrotron x-ray studies of the nematic (N) and the smectic-A (SMA) phases under non-equilibrium 'steady state' shear flow conditions. Under shear, the presence of SMA fluctuations leads to a novel flow-induced fluctuation force on the nematic director $\hat{n}$ which alters its equation of motion. This leads to rich behaviour where the nematic phase exhibits a sequence of regimes in which the orientational phase space (OPS) explored by $\hat{n}$ evolves as the N–SMA transition is approached. We directly observe the critical slowing down of the SMA order parameter fluctuations through the x-ray profiles, which give the intensity map of the time- and space-averaged OPS traversed by $\hat{n}$. Our data are consistent with the classical Ericksen–Leslie–Parodi theory of nematodynamics away from the immediate vicinity of the N–SMA transition temperature. Closer in, however, fluctuation effects dominate and a model of critical nematodynamics has to be considered. The experiments demonstrate that synchrotron scattering techniques may be used as effective structural probes of dynamical systems.

1. Introduction

The simplest liquid crystalline phases are the nematic (N) and smectic-A (SMA) phases. In the nematic phase, the rod-shaped molecules exhibit orientational order and point, on average, along a unique direction specified by a unit vector $\hat{n}$ called the director (see figure 1, lower part). The N–SMA transition corresponds to the onset of a one-dimensional mass density wave along the direction of $\hat{n}$. At equilibrium, the pretransitional SMA fluctuation clusters, which are measured by x-rays, grow in the nematic phase as one approaches the N–SMA transition and are ultimately responsible for the ordered SMA phase [1].

Using a high-resolution x-ray scattering spectrometer we have studied the microscopic structure of the nematic and SMA phases in 4-cyano-4′-octylbiphenyl (8CB) under non-equilibrium steady-state shear flow conditions. The presence of large fluctuations under shear flow leads to a novel flow-induced fluctuation force on the nematic director which then alters the equation of motion of $\hat{n}$ [2, 3]. We find that under shear flow as a function of decreasing temperature, the nematic phase exhibits a series of regimes where the orientational phase space (OPS) explored by $\hat{n}$ evolves as the N–SMA transition is

0953-8984/90/SA0365 + 07 $03.50

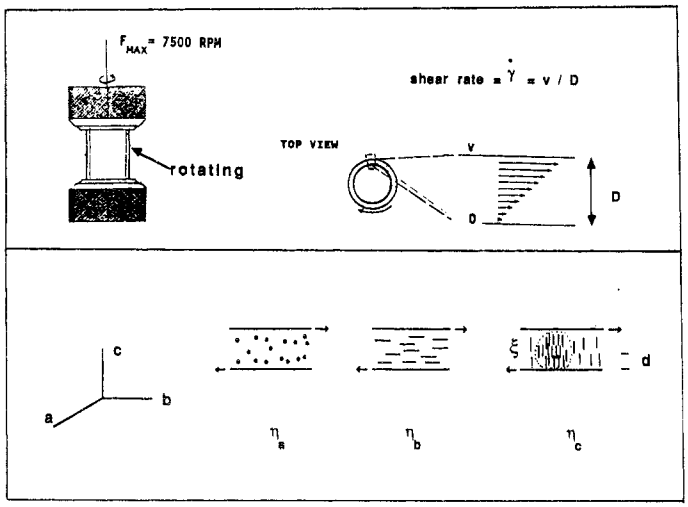

Figure 1. *Top*: (left) Couette x-ray shear cell; (right) simple shear flow field. *Bottom*: Three simple shear flow geometries for $\hat{n}$, with associated viscosities. For the c orientation, we show a SMA fluctuation cluster of size ξ.

approached. More specifically, the x-ray profiles which map out the time- and space-averaged OPS traversed by $\hat{n}$, allow us to observe directly the consequences of the flow-induced fluctuation force which are (i) the renormalization of one of the shear viscosities α_3, and (ii) the onset of a friction term which dampens the motion of $\hat{n}$ and keeps it confined to a plane normal to the flow direction. The renormalization of α_3 is directly due to the divergence of the fluctuation relaxation time τ, which corresponds to the critical slowing down of the SMA order parameter fluctuations.

2. Experimental details

Figure 1 shows the Couette x-ray shear cell consisting of two concentric cylinders where the outer cylinder rotates and the inner is fixed. A top view of the cell and the flow field (with shear rate $\dot{\gamma}$) experienced by the liquid crystal is shown in the top right of figure 1. The cell is temperature controlled to within ± 5 mK. The important distinguishing feature of our x-ray Couette cell is that it is sealed so that we are able to tilt and rotate the cell and map out the x-ray structure factor both in the shear plane and out of the shear plane. The details of the x-ray shear cell are described in a separate paper [4]. The experiments were conducted at the National Synchrotron Light Source (NSLS) on the Exxon beam line X-10A.

The three simple geometries that the nematic direction $\hat{n}$ may assume (bottom of figure 1) are referred to as the a, b and c orientations where each has an associated viscosity. The flow direction is along $\hat{b}$, the shear (∇v) direction along $\hat{c}$, and the neutral direction along $\hat{a}$.

3. Results

Figure 2 shows the shear rate versus temperature phase diagram and the rich sequence of regimes discovered in the nematic phase. At equilibrium for zero shear, 8CB

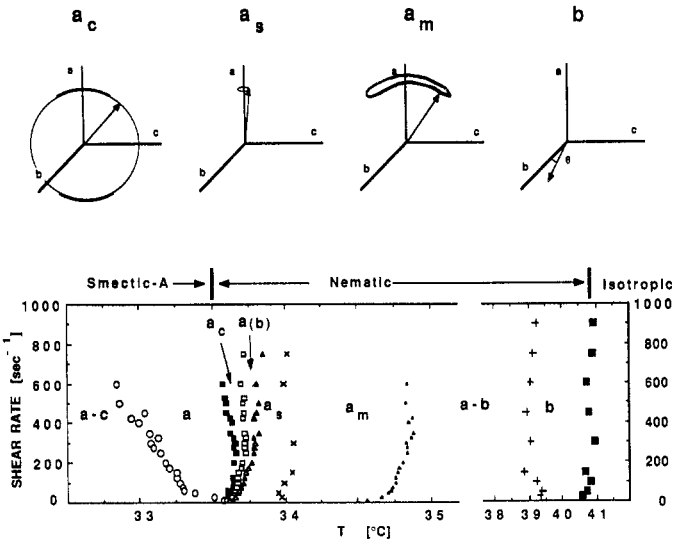

Figure 2. Shear rate versus temperature phase diagram for 8CB. The nematic shows six regimes distinguished by the orientational phase space explored by $\hat{\boldsymbol{n}}$ (shown schematically for four regimes at the top). The SMA phase shows two regimes.

exhibits an isotropic-to-nematic transition at $T_{IN} \simeq 40.5$ °C and a N-SMA transition at $T_{NA} \simeq 33.58$ °C. For finite shear, the evolution across regimes as a function of decreasing temperature is associated with the varying orientational phase space (OPS) explored by $\hat{\boldsymbol{n}}$ as the flow-induced fluctuation forces grow and alter its equation of motion. At the top of figure 2 we show schematics of the OPS occupied by $\hat{\boldsymbol{n}}$ for four of these regimes. We now give a brief description of each regime. A more detailed account is published separately [5].

The orientational state of $\hat{\boldsymbol{n}}$ is determined by the total torques acting on it. Under flow, these include the viscous and elastic torques [6], and the fluctuation torque due to the SMA fluctuation clusters [2, 3]. In our experiments, we are in the high shear limit where elastic torques are negligible. In the classical Ericksen–Leslie–Parodi (ELP) theory of nematodynamic [6], which considers the viscous and elastic torques, the viscosity coefficients α_2 ($\propto \eta_c$) and α_3 ($\propto \eta_b$) enter the equation of motion of the director $\hat{\boldsymbol{n}}$ and control the flow orientation of $\hat{\boldsymbol{n}}$. (Figure 1 defines η_c and η_b.) α_2 is always negative. Just below the isotropic-to-nematic transition temperature T_{IN}, α_3 is negative (with $|\alpha_3| \ll |\alpha_2|$) and ELP nematodynamics has a stable solution with $\hat{\boldsymbol{n}}$ lying in the (b–c) flow plane making a small angle $\theta = \tan^{-1}(\alpha_3/\alpha_2)^{1/2}$ with the b axis (this is the ***b*** region shown in figure 2, just below T_{IN}). As temperature is reduced the pretransitional SMA fluctuation clusters are expected to renormalize α_3, increasing it through zero and towards positive values [2, 3]. For $\alpha_3 > 0$, there is no stable solution with $\hat{\boldsymbol{n}}$ in the (b–c) shear plane. However, there is a solution where no torque is applied with $\hat{\boldsymbol{n}}$ pointing exactly along the $\hat{\boldsymbol{a}}$ direction out of the shear plane. This orientation is only *marginally stable* and if we consider $\hat{\boldsymbol{n}}$ close to $\hat{\boldsymbol{a}}$, where $\hat{\boldsymbol{n}} = (n_b, n_c, 1)$ with n_b, $n_c \ll 1$, the modified ELP nematodynamics [2] (which considers the flow-induced fluctuation forces to lowest order in $(\gamma\dot{\tau})$ by renormalizing α_3), yields a simple equation of motion:

$$\ddot{n}_b + \omega_0^2 n_b = 0$$
$$n_c = (-\gamma_1/\dot{\gamma}\alpha_2)\dot{n}_b \tag{1}$$

where $\omega_0^2 = \dot{\gamma}^2[\alpha_3^R(-\alpha_2)]/\gamma_1$. Here γ_1 is one of the five nematic viscosities and the fluctuation renormalized viscosity is given by

$$\alpha_3^R = \alpha_3 + 4\pi^4\left(\frac{k_B T}{\xi d^2}\right)\tau.$$

(d and ξ are the layer spacing and correlation size of a fluctuation cluster, as shown in figure 1.) Equation (1) describes a simple coupled harmonic oscillator motion for n_b and n_c with precession frequency ω_0. Note, however, that because there is no damping term in (1), the solution is marginally stable and $\hat{\boldsymbol{n}}$ will perform a precessing motion about the a axis but can also wander (due to thermal or hydrodynamic noise) between different amplitude states for n_{b0} and n_{c0}. That is, solutions to (1) have the simple precession form $n_b = n_{b0}\cos\omega_0 t$, $n_c = n_{c0}\sin\omega_0 t$, with $n_{b0}/n_{c0} = (-\alpha_2/\alpha_3^R)^{1/2}$. Thus we expect a regime where $\hat{\boldsymbol{n}}$ wobbles about the $\hat{\boldsymbol{a}}$ direction. We see from the phase diagram of figure 2 that our experiments show a crossover from the $\boldsymbol{b}$ regime (just below T_{IN}), to a marginally stable regime labelled a_m, where in fact, the direction exhibits a wobbly precessing motion with $\hat{\boldsymbol{n}}$ tipping off the a axis. In the intermediate regime labelled a–b, there are substantial boundary layers with the b orientation. Thus, far away from the immediate vicinity of T_{NA}, our data are consistent with the modified-ELP model of nematodynamics. However, as we see from figure 2, three other regions (labelled a_s, $a(b)$ and a_c) appear, and we shall see that a recently developed model of critical nematodynamics is in reasonable agreement with much of the data [3].

As we further lower the temperature we cross over from the a_m to the a_s regime (s for stable). In this regime, $\hat{\boldsymbol{n}}$ is confined to a small cone about the $\hat{\boldsymbol{a}}$ direction which appears to be a stable solution for $\hat{\boldsymbol{n}}$. Further lowering of the temperature results in a crossover across two more distinct regimes labelled $a(b)$ and a_c in figure 2 before the SMA phase is reached. (In the SMA phase, $\hat{\boldsymbol{n}}$ initially points along the a axis but at lower temperatures crosses into a regime where SMA domains with both the $\hat{\boldsymbol{a}}$ and $\hat{\boldsymbol{c}}$ orientations coexist (figure 2).) We now describe the final three regimes in the N phase.

To understand the a_s regime we need to go beyond the modified-ELP nematodynamics and to consider what we shall call critical nematodynamics, which includes the effects of the flow-induced fluctuation force more completely [3]. In critical nematodynamics the ELP equation of motion (1) is modified with the appearance of a new friction term. The equation of motion then becomes

$$\ddot{n}_b + 1/\dot{\tau}_N\, n_b + \omega_0^2 n_b = 0$$
$$n_b = -\frac{\gamma_1}{\dot{\gamma}\alpha_3^R}\dot{n}_c \tag{2}$$

which corresponds to a damped coupled harmonic oscillator equation with damping rate

$$\frac{1}{\tau_N} = \frac{\pi^4}{3\gamma_1}\left(\frac{k_B T}{\xi d^2}\right)(\dot{\gamma}\tau)^2.$$

Since this is a higher-order term than the precession term, it will become important only in the vicinity of T_{NA} where fluctuations grow very large and τ tends to diverge. For most of the temperature range, $\omega_0 > 1/\tau_N$. Thus in the a_s regime $\hat{\boldsymbol{n}}$ undergoes an *undamped* precessing motion and is confined to a small cone about the $\hat{\boldsymbol{a}}$ direction.

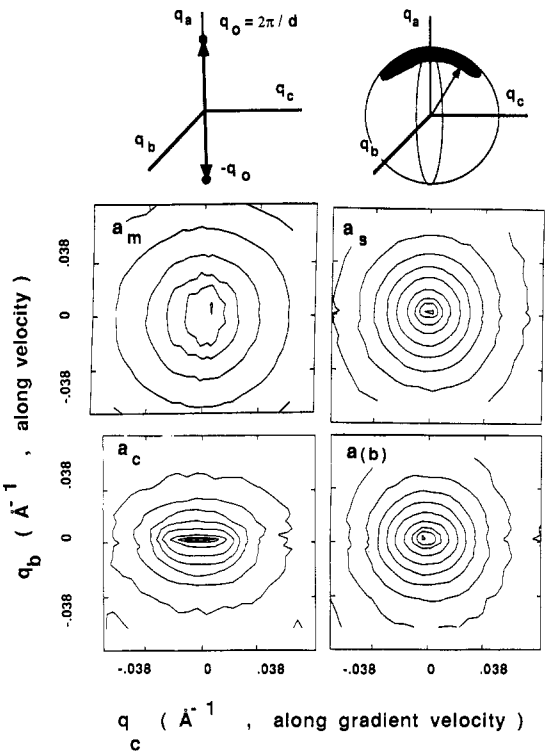

Figure 3. *Top*: (left) Diffuse x-ray spots for $\hat{\boldsymbol{n}}$ pointing along $\hat{\boldsymbol{a}}$; (right) diffuse x-ray patch of a sphere of radius q_0 due to a corresponding distribution of decreasing temperature (shown for four regimes). The evolution in the elliptical shapes is due to the renormalization of α_3^R which arises from the critical slowing down of the SMA order parameter fluctuations.

In the $a(b)$ regime, we find a *bulk* coexistence of regions of the sample where $\hat{\boldsymbol{n}}$ points along $\hat{\boldsymbol{a}}$ and regions where $\hat{\boldsymbol{n}}$ points (approximately) along $\hat{\boldsymbol{b}}$ in the $(b\text{–}c)$ shear plane. That is, regions of the sample have *re-entered* the high-temperature $\boldsymbol{b}$ orientation (see figure 2). The existence of a coexistence regime for the temperature range near T_{NA} where $\dot{\gamma}\tau(\xi/d) > 1 > \dot{\gamma}\tau$ has been anticipated theoretically, and has been attributed to the anisotropic suppression of SMA fluctuations due to flow [3].

In the final a_c regime in the nematic phase just above T_{NA} (figure 2), $\hat{\boldsymbol{n}}$ points mostly along $\hat{\boldsymbol{a}}$ but undergoes a non-uniform precessing motion tumbling all the way towards the $\hat{\boldsymbol{c}}$ direction. We argue below that this behaviour for $\hat{\boldsymbol{n}}$ arises from the divergence of α_3^R/α_2 as T approaches T_{NA}. Furthermore, in this regime, $\hat{\boldsymbol{n}}$ is confined to the $(a\text{–}c)$ plane with no $\hat{\boldsymbol{b}}$ component because of the presence of the friction term (in equation (2)) which applies a torque on $\hat{\boldsymbol{n}}$, pushing it towards the $(a\text{–}c)$ plane [3].

The growth of the coefficients (e.g. α_3^R, and the friction term) arising from the flow-induced fluctuation forces, with decreasing temperature, is reflected directly in the x-ray intensity scattering profiles. For a uniform sample with $\hat{\boldsymbol{n}} = \hat{\boldsymbol{a}}$, the x-ray scattering profile gives diffuse spots at $\boldsymbol{q} = \pm q_0\hat{\boldsymbol{n}}$ in reciprocal $\boldsymbol{q}$-space, as shown at the top left of figure 3. Therefore, the diffuse spots *point* along $\hat{\boldsymbol{n}}$ and give us the orientation of the director. For a distribution of $\hat{\boldsymbol{n}}$ which is determined by the total forces acting on $\hat{\boldsymbol{n}}$, the diffuse scattering would now be on a corresponding 'patch' of a sphere of radius q_0. (This

is shown at the top right of figure 3). The map of the x-ray intensity levels thus is used as a probe of the director orientation distribution function $W(\hat{\boldsymbol{n}})$. The x-ray intensity is given by

$$I(\boldsymbol{q}) \sim \int \mathrm{d}n \, \langle W(\hat{\boldsymbol{n}}) \rangle S(\boldsymbol{q}, \hat{\boldsymbol{n}})$$

where $S(\boldsymbol{q}, \hat{\boldsymbol{n}})$ is the scattering for a given $\hat{\boldsymbol{n}}$, and the average $\langle\ \rangle$ is over time and space.

To obtain a sensible functional form for the distribution function $\langle W(\hat{\boldsymbol{n}}) \rangle$, we consider the equation of motion in the limit where $\omega_0 \gg 1\tau_N$, which is correct for most of the nematic range except for T within a few mK of T_{NA}. Equation (1), which includes the renormalization of α_3^R, is then a good approximation for the equation of motion of $\hat{\boldsymbol{n}}$. This equation describes a simple precession mode:

$$n_b = n_{b0} \cos \omega_0 t \qquad n_c = n_{c0} \sin \omega_0 t$$

which satisfies the equation of an ellipse:

$$n_b^2/n_{b0}^2 + n_c^2/n_{c0}^2 = 1 \tag{3}$$

with

$$n_{b0}/n_{c0} = \left(\frac{-\alpha_2}{\alpha_3^R}\right)^{1/2}$$

the ratio of the axes. The nematic director jumps between different amplitudes n_{b0}, n_{c0} due to noise but always precesses with the same ratio of amplitudes. Thus, a sensible functional form for the distribution function would be

$$\langle W(\hat{\boldsymbol{n}}) \rangle \sim \exp[\, -(n_b^2 \sigma_b^2 + n_c^2 \sigma_c^2)]$$

with $\sigma_b/\sigma_c = n_{b0}/n_{c0}$. Therefore, the x-ray intensity levels should also be elliptical.

Figure 3 shows equal intensity contour plots in the (b–c) shear plane (with $q_a = q_0$), in the four regimes above T_{NA}. The elliptical shapes are self-evident. As a function of decreasing temperature, in the a_m regime the major axis is along $\hat{\boldsymbol{b}}$ since $\alpha_3^R < -\alpha_2$, while with increasing α_3^R, the shape becomes almost circular (figure 3, a_s regime) and elliptical again (in the $a(b)$ regime) but not with the major axis along $\hat{\boldsymbol{c}}$ because $\alpha_3^R > -\alpha_2$. Finally, the contours become extremely anisotropic in the a_c regime with $\alpha_3^R \gg -\alpha_2$. In this final regime, a small amplitude fluctuation n_{bo} results in a precession path with a large n_{c0} amplitude which then causes the director to traverse the (a–c) plane. Large amplitude fluctuations along n_{b0} are not seen because of the friction term which confines $\hat{\boldsymbol{n}}$ to the (a–c) plane.

Thus, the x-ray profiles allow us to directly observe the divergence of $\alpha_3^R \propto \tau/\xi$, which is directly related to the critical slowing down of the SMA order parameter fluctuations. Over the temperature range spanning the last four regimes, we find that α_3^R increases by a factor of about 400 [5].

4. Conclusions

In summary, we have seen that the flow-induced fluctuation forces on the nematic director lead to a rich sequence of regimes where the orientational phase space traversed by $\hat{\boldsymbol{n}}$ evolves as the N–SMA transition is approached. Our data are consistent with the ELP

theory of nematodynamics away from the critical regime. Near T_{NA}, critical nematodynamics has to be invoked. Finally, the experiments demonstrate that synchrotron scattering techniques may be used as effective structural probes of dynamical systems.

Acknowledgment

The National Synchrotron Light Source, Brookhaven National Laboratory, is supported by the US Department of Energy.

References

[1] Davidov D, Safinya C R, Kaplan M, Dana S S, Schaetzing R, Birgeneau R J and Litster J D 1979 *Phys. Rev.* B **19** 1657
[2] McMillan W L 1974 *Phys. Rev.* A 1720
Janig F and Brochard F 1974 *J. Physique* **35** 301
[3] Bruinsma R F and Safinya C R 1990 *Macromolecular liquids* C R Safinya, S A Safran and P A Pincus (eds) (Materials Research Society Publishers **177**) p 153
Bruinsma R F and Safinya C R 1990 *Phys. Rev.* A (submitted)
[4] Plano R J, Safinya C R and Wenzel L 1990 *Rev. Sci. Instrum.* (submitted)
[5] Safinya C R, Sirota E B and Plano R J 1990 *Phys. Rev. Lett.* (submitted)
[6] Ericksen J L 1960 *Arch. Ration. Mech. Anal.* **4** 231
Leslie F M 1966 *Quart. J. Mech. Appl. Math.* **19** 357
Parodi O 1970 *J. Physique* **31** 581